

Microwave Active Thermography (MIRT) for rebars detection and evaluation in reinforced concrete structures

by Szymanik, B*.; Keo, S.A.**; Brachelet, F.***; Defer, D.***

*Center for Electromagnetic Fields Engineering and High-Frequency Techniques, Faculty of Electrical Engineering, West Pomeranian University of Technology, 70-310 Szczecin, Poland

**ESTP–Grande Ecole D'ingénieurs de la Construction, 9-11 Rue Sully, 21000 Dijon, France

***Univ. Artois, IMT Nord Europe, Junia, Univ. Lille, ULR 4515, Laboratoire de Génie Civil et géo-Environnement (LGCgE), 62400 Béthune, France

Abstract

This study will propose the utilization of active infrared thermography with microwave excitation for the identification and assessment of reinforcement bars in concrete structures. In the first stage, an numerical modelling approach will be presented. Prepared numerical model is composed of a microwave source, a broadband antenna and a concrete structure with a selected arrangement of reinforcing bars. Numerical modeling will be used to determine the optimal measurement methodology. The numerical results will be then validated through an experimental approach.

1. Introduction

Reinforced concrete has been a generally prevalent construction material for more than a century, despite the fact that structures made of this material frequently experience various forms of damage and deterioration as a result of diverse causes and exposure circumstances. Consequently, building code regulations necessitate regular inspections in most countries. Typically, these tests should be performed once the concrete has solidified and without causing any harm to the structure. Therefore, nondestructive testing procedures (NDTs) are frequently employed for this assessment. Reinforced concrete testing encompasses various crucial features that hold practical significance:

- Evaluating the measurements of structural components and identifying any damage or imperfections, such as empty spaces, fractures, and foreign materials. The most widely used non-destructive testing (NDT) methods include ultrasonic sensors and ground penetrating radar [1 - 9]. Both methods exhibit high speed and reliability, but, the outcomes acquired are challenging to comprehend. Active and passive thermography can be utilized for examining the internal composition of concrete. However, in practical applications, these techniques are primarily employed for identifying surface faults or plaster problems, as they have some limits [9, 10].
- Assessment of the location and corrosion reinforcement. The most suitable options in this case are electromagnetic techniques, including radiography (a highly effective but challenging and hazardous method for operators) [11 - 14], eddy current sensors (a promising method that enables both detection and identification of reinforcement) [15 - 17], and impedance tomography, which, unlike the aforementioned methods, requires direct contact.
- Moisture evaluation. The most often employed techniques include impedance tomography [18 - 20], thermography, and several chemical approaches.

Active thermography requires the use of an external energy source to create a temperature contrast within the examined material. Conventional heating technologies, such as halogen lights, flash lamps, infrared radiators, and hot air, are often ineffective for heating big concrete structures. Our work suggests the utilization of microwave heating. In literature, microwave heating is mostly employed to expedite the curing process, decontaminate cement, and facilitate concrete drilling or melting. In this study, we suggest the utilization of microwaves as the energy source for infrared thermography. The primary benefit of microwave heating lies in its volumetric nature. This approach is characterized by its rapidity, as a specific volume of the specimen is heated instantaneously. Conversely, for this unconventional energy source, the heating ratio relies not only on the thermal characteristics of the material, but also on certain electrical qualities. Furthermore, a noteworthy occurrence is witnessed when microwaves interact with metal. The heating process is significantly restricted due to the exceptionally small value of the penetration depth. This phenomena will be illustrated in both numerical simulations and experiments.

Our previous investigation in this topic [21 – 24] include the research on the structures with a single steel rebar using both – numerical and experimental approaches, as well as the sole experimental approach to the multiple rebars structure, including the analysis of the influence of the diffraction and the interference phenomenon on the heating patterns observable at the sample surface. In this study we would like to present the extensive numerical approach to the more complex system of several rebars in the concrete structure. The analysis of the temperature change dynamics will be presented. The results will be validated by the experiments.



2. Materials and Methods

In this section, we present the numerical models and the utilized experimental setups. The numerical analysis was performed using the finite element method (FEM) in a COMSOL computing environment (<https://www.comsol.com/>). In the subsequent section, all the elements of the designed numerical models are presented.

2.1. Numerical models

The numerical models were designed with a broadband horn aluminium antenna and a concrete block including eight steel reinforcing bars (Fig. 1). The dimensions of the block were slightly decreased compared to the actual object tested in the experiment. However, it was decided to simulate the object using multiple reinforcing bars to examine potential alterations in the temperature distribution caused by the presence of numerous steel objects within the concrete block. The modeled concrete block had dimensions of 800 x 800 x 65 mm. Each steel rod had a diameter of 12 mm and the distance between the centers of the rods was 100 mm. The thickness of the concrete cover above the bars on the antenna side was 15 mm.

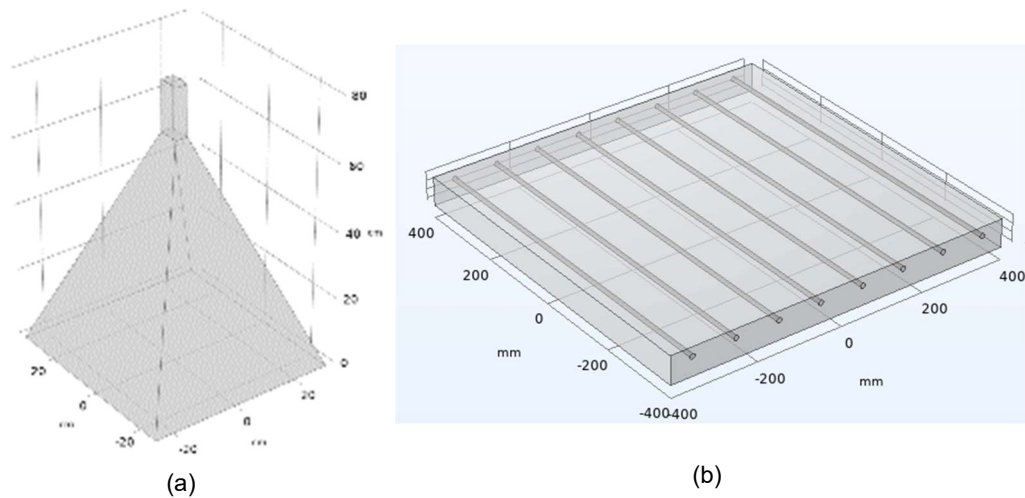


Fig. 1. Elements of the geometry utilized in the numerical modelling. (a) the broadband horn antenna, (b) the concrete block with steel reinforcement bars

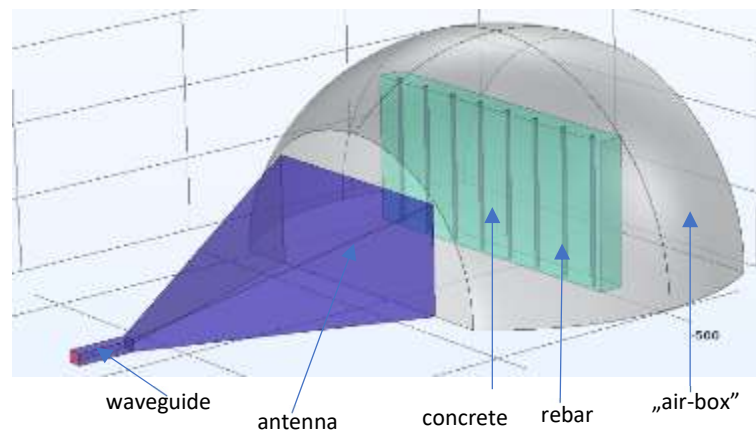


Fig. 2. The model geometry

Figure 2 depicts the entirety of the geometry that was examined. As depicted, computations were performed on half of the entire geometry. This action was taken due to the presence of symmetry in the current configuration of the system. The sample was placed at a distance of 40 cm from the antenna. An air-filled sphere was placed around the sample. Three scenarios were examined during the numerical analysis (Fig. 3):

- The sample located in front of the antenna at an angle of 0° (Fig. 3 (a))

- The sample located in front of the antenna at an angle of 30° (Fig. 3 (b))
- The sample located in front of the antenna at an angle of 45° (Fig. 3 (c))

First scenario (sample at an angle of 0°) is not possible to be implemented experimentally due to the fact that the thermal camera must be able to record an image on the sample surface, however, such a scenario was also taken into account in the numerical analysis in order to estimate the influence of the sample position angle relative to the antenna on the final temperature distribution on the concrete surface.

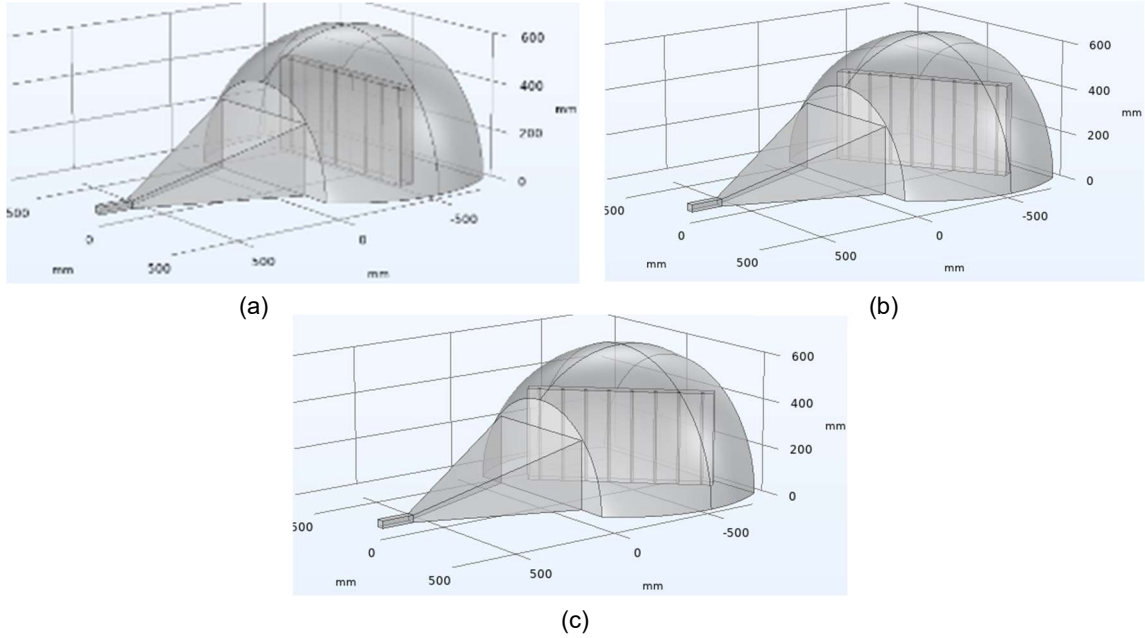


Fig. 3. Three analysed numerically scenarios: (a) the sample located in front of the antenna at an angle of 0°, (b) the sample located in front of the antenna at an angle of 30°, (c) sample located in front of the antenna at an angle of 45°

The numerical models were prepared in the commercial computing environment - COMSOL, in particular using Heat Transfer (HT) and Electromagnetic Waves (EMW) modules to fully analyze the phenomena of microwave heating. The propagation of an electromagnetic wave is defined as follows [26]:

$$\nabla^2 \mathbf{E} + (\mu\epsilon\omega^2 - i\mu\sigma\omega)\mathbf{E} = 0 \quad (1)$$

where μ denotes the magnetic permeability, ϵ is the electric permittivity, σ represents the electric conductivity, ω is the angular frequency, and \mathbf{E} is the electric field vector.

The heat flow is characterized here by the equation [25]:

$$\rho C_p \left(\frac{\partial T}{\partial t} + \nabla T \right) + \nabla \mathbf{q} = Q \quad (2)$$

where ρ is the material density, C_p denotes the material heat capacity, \mathbf{q} is the heat flux associated with the convection phenomenon, T is the temperature, and " Q " denotes the external heat source.

And the external heat source is equal to the resistive heat generated by the electromagnetic field, which is described as follows [26]:

$$Q = 1/2 \text{Re}((\sigma - j\omega\epsilon)\mathbf{E} \cdot \mathbf{E}^*) \quad (3)$$

where Re indicates the real part of the value. An electromagnetic wave was produced through the application of the port boundary condition on a specific wall within the waveguide. Here, the assumed mode was TE₁₀, the frequency was equal to 2.45 GHz and the total power was set to 600 W. The energy was transmitted in the continuous manner for 300 s.

In the Table 1 all the used material parameters are gathered:

Table 1. Thermal and electrical parameters of chosen materials used in the numerical model

	Aluminum	Steel	Concrete
Heat capacity: C_p [J/(kg*K)]	NA	475	880
Density: ρ [kg/m ³]	NA	7850	2300
Relative permittivity: ϵ	1	1	8.5-0.86j
Thermal conductivity: k [W/(m*K)]	NA	44.5	0.8
Electrical conductivity: σ [S/m]	3.77e7	4.032e6	0.1
Relative permeability: μ	1	1	1

2.2. Experimental Setup and Specimens

Two experimental campaigns were carried out with a reinforced concrete (RC) wall sample as in the numerical simulation. On the top of the RC wall, there are extremities of the steel bars inside the wall, which allow to locate the real position of each steel bar. The experimental setup of the tests are shown in Figure 1. In accordance with safety regulations, the tests were conducted inside a microwave protection enclosure which was already used in previous works [1–3].

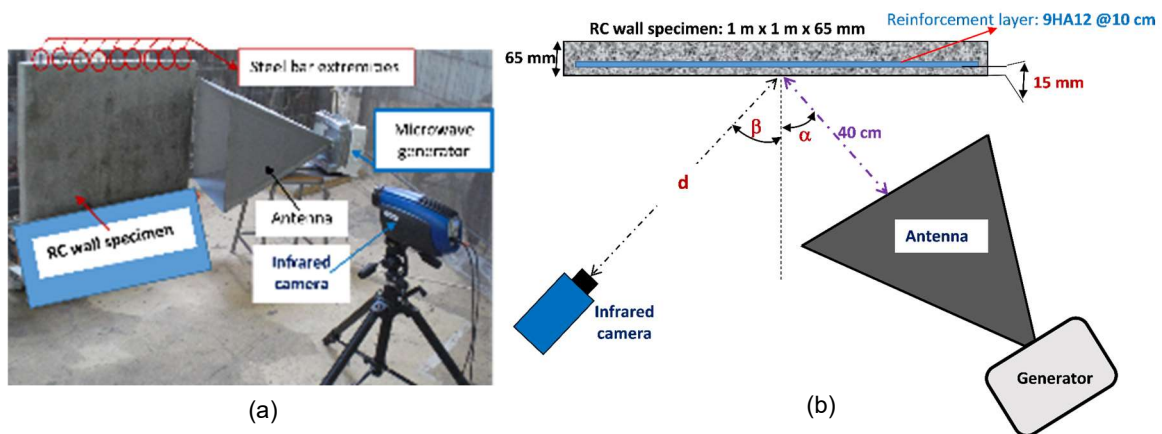


Fig. 4. (a) Experimental setup inside the protective enclosure, (b) Experimental set up of the microwave thermography tests with both cases of antenna direction (α)

The 2.45 GHz microwave system, as in the numerical model, was used to heat the RC wall sample with an average power of 600 W for 300 s (modulation heating mode). Nine steel bars of 12 mm diameter were placed at every 100 mm inside the RC wall. The concrete cover for the side exposed to the antenna is 15 mm. The pyramidal horn antenna was placed at 40 cm from the sample in two cases of direction (α): 30° direction, and 45° direction. An infrared camera was used to record thermograms with a frame rate of 5 images per second. Two different positions of the infrared camera were used for both cases of the antenna direction (so that the whole part of the wall sample can be observed). The infrared camera was placed at 2.11 m (d) from the sample in 45° direction (β) when the antenna was in 30° direction (α), and at 2.32 m (d) from the sample in 30° direction (β) when the antenna was in 45° direction (α). Fig. 5 shows the output signal of the microwave detected by a sensor. At the average power of 600 W, it is the pulse train with a period of 30 s and pulse duration of 23 s. In each slot of the train, there is a modulation period of 200 ms and 100 ms of pulse duration.

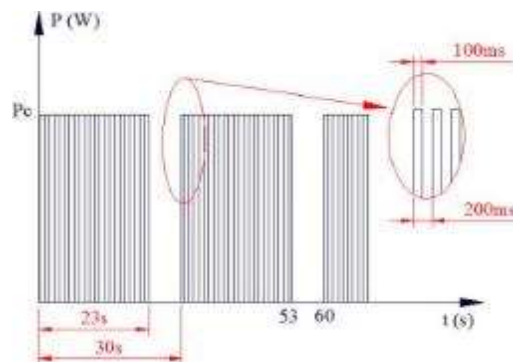


Fig. 5. Generated microwave signal

3. Numerical Modelling Results

In this section, the results of the numerical modeling for all the previously introduced scenarios will be presented. First, we will present the raw numerical results to assess their quality, and subsequently, we will compare them with the data from the experiments. Figure 6 depicts the outcome of microwave heating on the reinforced concrete at the specific time interval ($t = 300$ s). The relative position of the sample with respect to the antenna aperture significantly affects the resulting temperature distribution on the surface of the tested concrete.

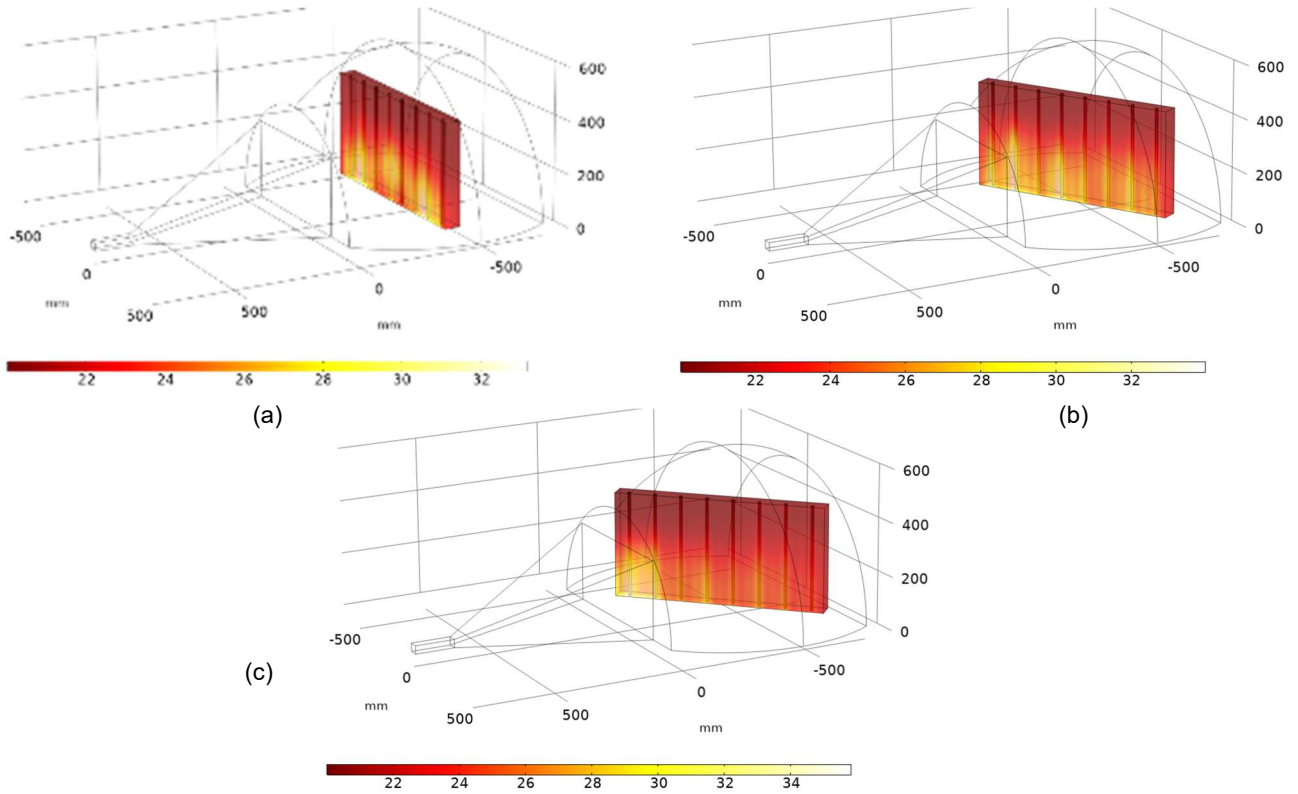


Fig. 6. Exemplary numerical results for three analysed scenarios: (a) the sample located in front of the antenna at an angle of 0° , (b) the sample located in front of the antenna at an angle of 30° , (c) sample located in front of the antenna at an angle of 45°

Since the electromagnetic wave's ability to penetrate steel at GHz frequencies is limited to micrometers (specifically around $4 \mu\text{m}$ in our case), the steel bars should not experience considerable heating from microwaves. The lower wall of the concrete block is clearly visible in the Figure 7. It is evident that the concrete is heated, and the presence of the reinforcing bar restricts the heated area, resulting in warmer regions around the bars (above them).

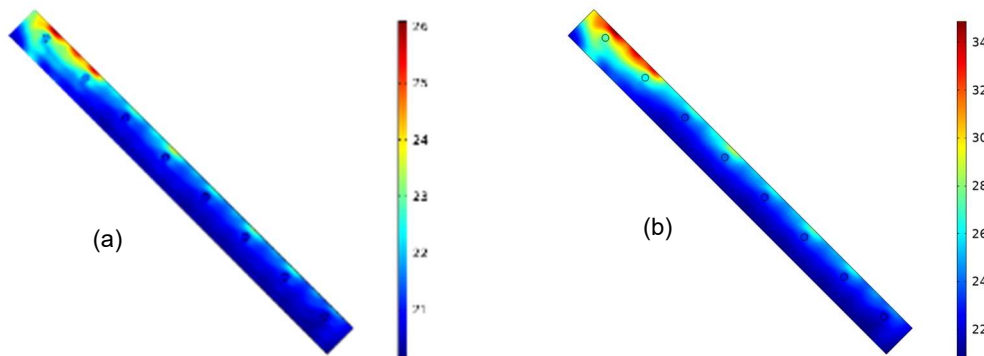


Fig. 7. The lower side of the concrete block with visible steel rebar, depicted for 45° scenario. a) after 100 s of heating, b) after 300 s of heating

Figure 8 displays the outcomes of numerical simulation for every scenario at specific time intervals. From the raw images, it is evident that the temperature distribution is marked by the presence of stripes, which are clearly associated with the reinforcing bars. However, accurately determining the exact position of the bars in these raw images is challenging because the temperature distribution is predominantly affected by uneven heating caused by the ceratin radiation pattern of the antenna and the samples being oriented at an angle to the antenna.

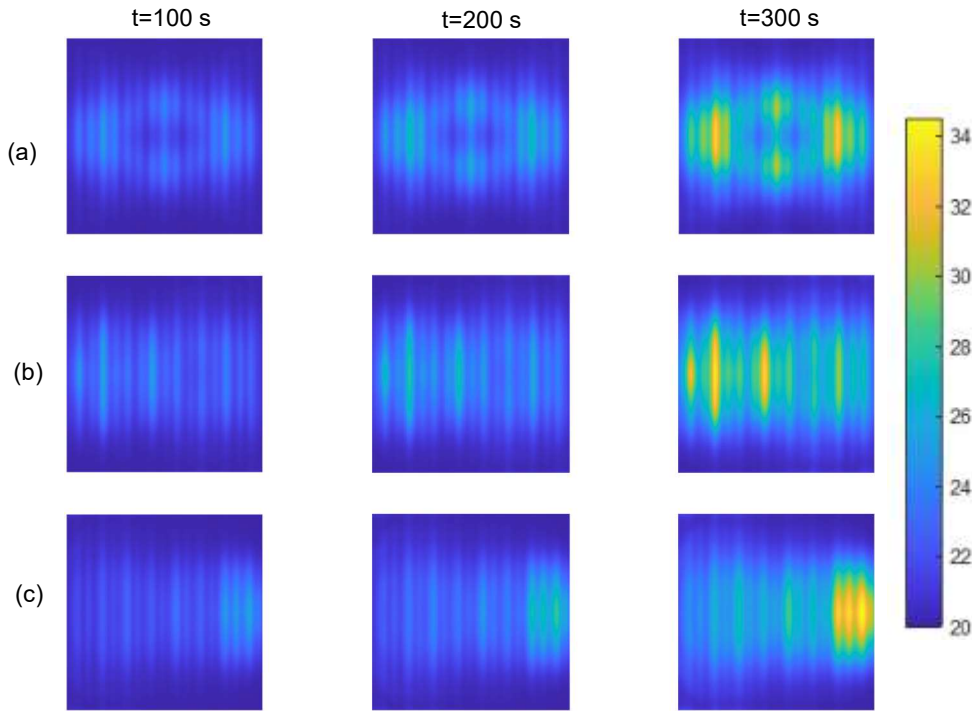


Fig. 8. Temperature distribution at the sample's surface for three time steps: 100, 200 and 300 s of heating, presented for three analysed scenarios: (a) the sample located in front of the antenna at an angle of 0° , (b) the sample located in front of the antenna at an angle of 30° , (c) sample located in front of the antenna at an angle of 45°

To eliminate the noticeable impact of the antenna radiation pattern and the sample orientation in relation to the aperture, we suggest employing a trend removal technique that relies on median filtering. The idea is to use median filtering with a large mask. Finally, the obtained data is subtracted from the original image. This process is shown in Figure 9.

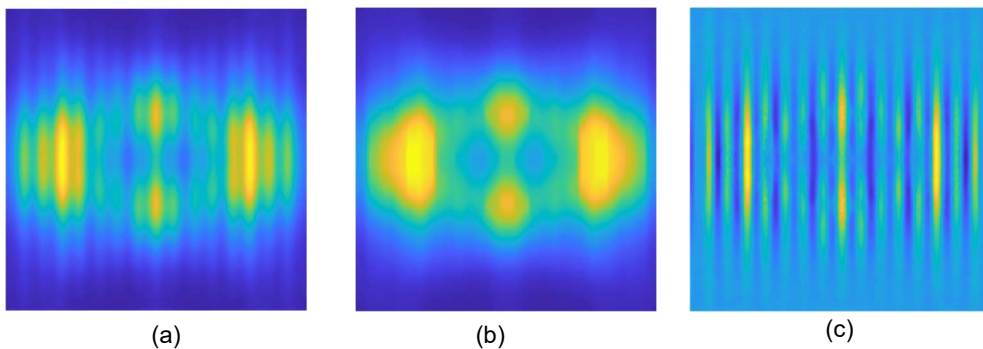


Fig. 9. Visualization of the background removal method based on median filtering, shown for the chosen case. (a) original data, (b) data after median filtering with large mask, (c) results of subtraction (a,b).

Figure 10 presents the results of previously mentioned trend removal technique for chosen time step (300 s of heating) for all the analysed scenarios.

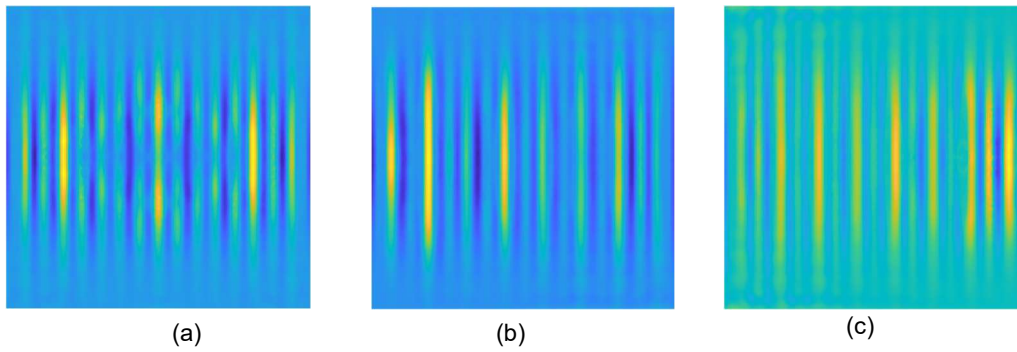


Fig. 10. The effect of trend removal, shown for three analysed scenarios: (a) the sample located in front of the antenna at an angle of 0° , (b) the sample located in front of the antenna at an angle of 30° , (c) sample located in front of the antenna at an angle of 45°

In order to demonstrate the potential for selecting the position of reinforcing bars, a graph showing a linear temperature distribution along the chosen line using the data from Figure 9 was created. The findings are displayed in the Figure 11. The gray rectangles depict the precise positioning of the steel bars. It is evident that the temperature maxima in all situations are directly correlated with the presence of the bars. However, it is evident, especially in scenario 0° (as shown in the Figure 11 (a)), that apart from the peaks associated with the presence of the bar, there are also other peaks present between the bars. The significant magnitudes of the extra peaks pose a challenge in identifying the bars. The amplitudes of the peaks for scenarios 45° and 30° are significantly smaller, particularly for case 30° as seen in the Figure 11 (b). This enables accurate identification of the positions of all rods.

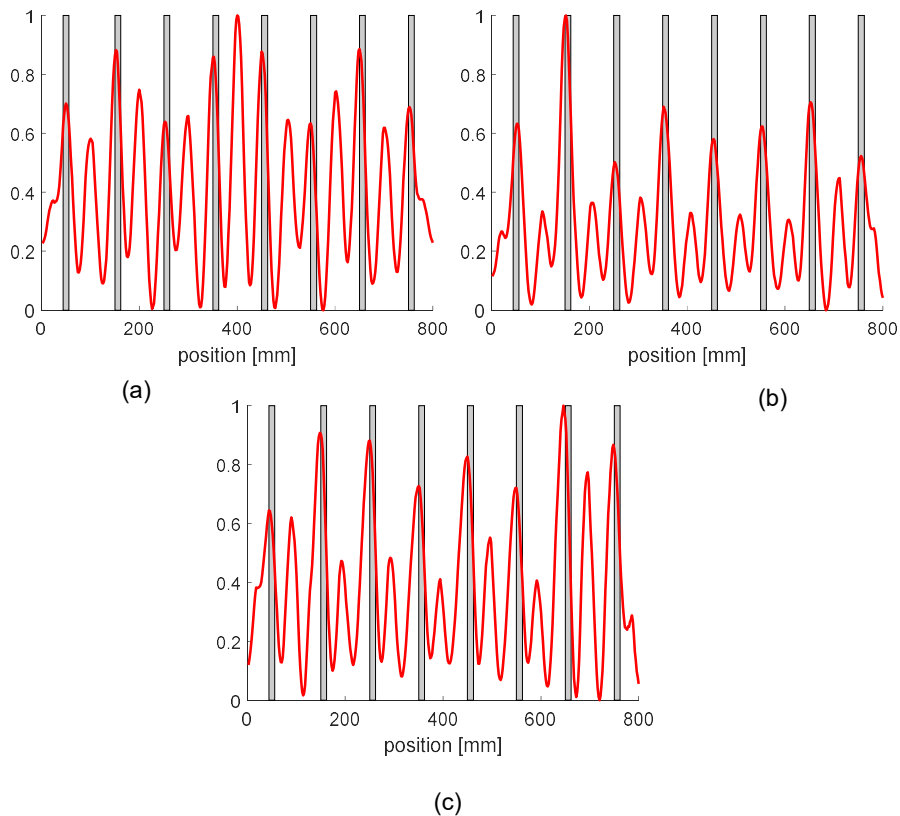


Fig. 11. Temperature distributions plotted along the chosen line of thermograms after trend removal for all the analysed scenarios: (a) the sample located in front of the antenna at an angle of 0° , (b) the sample located in front of the antenna at an angle of 30° , (c) sample located in front of the antenna at an angle of 45°

4. Experimental Results

This chapter will present the results of experiments carried out in accordance with the methodology discussed in chapter 2.2. The Figure 12 shows raw measurement results for two experimentally analysed scenarios: sample at an angle of 30° and 45°.

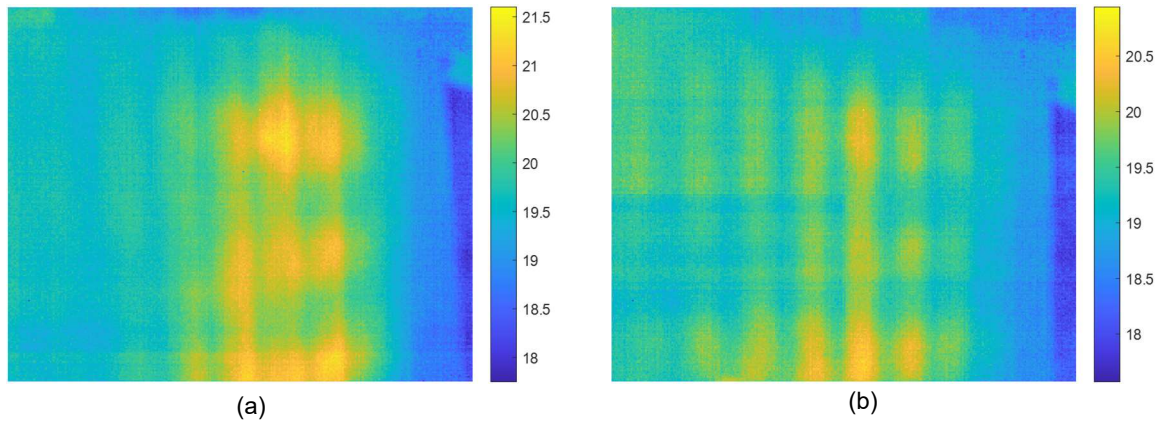


Fig. 12. Raw experimental results shown for chosen time step – 300 s: (a) the sample located in front of the antenna at an angle of 30°, (b) sample located in front of the antenna at an angle of 45°

Subsequently, the acquired images from the experiment were selectively trimmed to display solely the temperature distribution on the surface of the tested material. Figure 13 displays thermograms for both examined scenarios at three specific time points. Just like in case of the numerical data, also here the temperature distribution exhibits stripes that correspond to the presence of steel reinforcing bars. The presence of uneven heating can be observed, which is caused by the radiation characteristic of the antenna and the positioning of the sample in relation to the aperture.

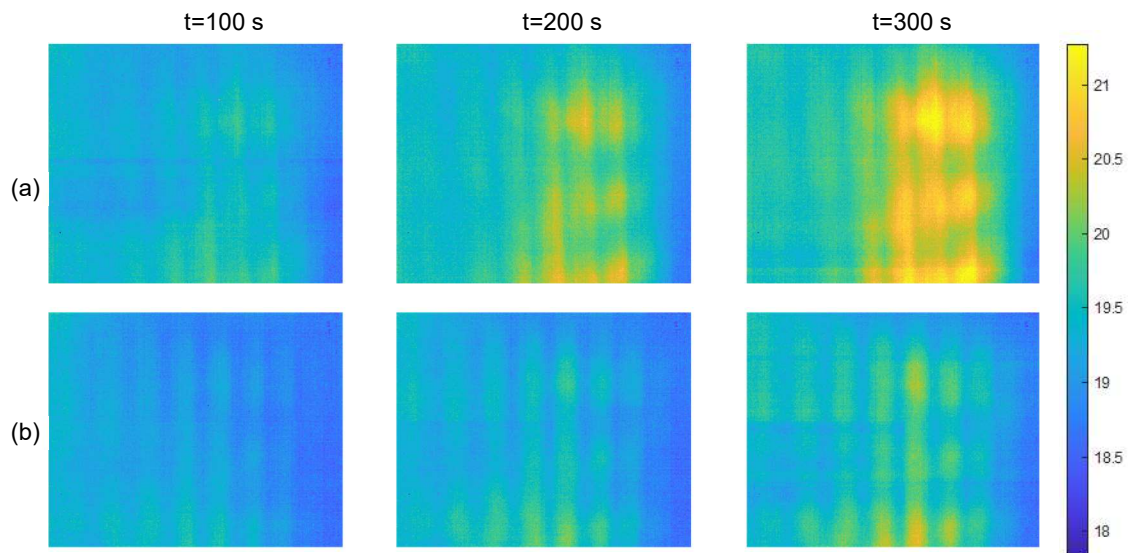


Fig. 13. Temperature distribution at the sample's surface for three time steps: 100, 200 and 300 s of heating, presented for two analysed scenarios: (a) the sample located in front of the antenna at an angle of 30°, (b) sample located in front of the antenna at an angle of 45°

Similar to numerical data, the experimental data underwent the trend reduction technique outlined in the previous section. This enabled the identification of local temperature peaks linked to the presence of steel reinforcement bars. The results underwent an extra process of average filtering to eliminate any unwanted noise. The completed outcomes are depicted

in the Figure 14. Similarly, to identify the reinforcing bars, the temperature distribution was shown along the chosen line. For scenario 45°, 8 reinforcing bars were accurately identified.

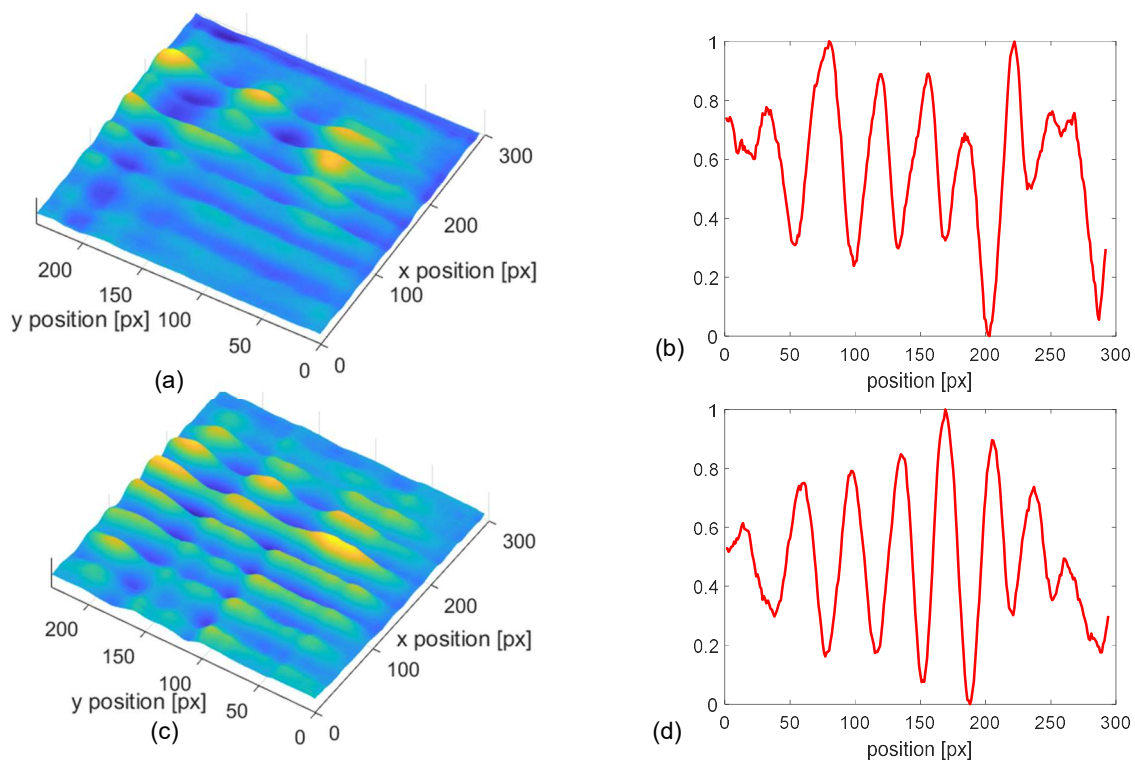


Fig. 14. The experimental data after trend removal (3D visualisation and temperature distribution along the chosen line), presented for two analysed scenarios: (a, b) the sample located in front of the antenna at an angle of 30°, (c, d) sample located in front of the antenna at an angle of 45°

5. Conclusions and Further Work

This work aimed to offer a comprehensive numerical methodology for analyzing the intricate network of many reinforcement bars in a concrete structural sample. Throughout the research, an investigation was conducted on the dynamics of temperature change. This included the presentation of a strategy for eliminating trends and a method for pinpointing the location of rebars. In order to validate all of the findings, experiments were conducted. The MIRT method shows promising indications of being a reliable approach for detecting and evaluation the rebars. Unlike the experiments that employed modulated heating, the numerical modeling method employed continuous heating. Considering this, the temperature values in the two cases are not the same. Conducting a qualitative analysis of the results was still feasible.

REFERENCES

- [1] Sakata, Y.; Ohtsu, M. Crack evaluation in concrete members based on ultrasonic spectroscopy. *ACI Mater. J.* **1995**, *92*, 686–698.
- [2] Schickert, M. Ultrasonic NDE of concrete. In Proceedings of the 2002 IEEE Ultrasonics Symposium, Munich, Germany, 8–11 October 2003; pp. 739–748.
- [3] Lorenzi, A.; Tisbierck, F.T.; Silva, L.C.P. Ultrasonic Pulse Velocity Analysis in Concrete Specimens. In Proceedings of the IV Conferencia Panamericana de END, Buenos Aires, Argentina, 22–26 October 2007.
- [4] Clayton, D.A. Nondestructive Evaluation of Thick Concrete Structures. In Proceedings of the International Symposium Non-Destructive Testing in Civil Engineering (NDT-CE), Berlin, Germany, 15–17 September 2015.
- [5] Al-Qadi, L.; Lahour, S. Ground Penetrating Radar: State of the Practice for Pavement Assessment. *J. Mater. Eval.* **2004**, *42*, 759–763.

- [6] Morcoux, G.; Erdogmus, E. *Use of Ground Penetrating Radar for Construction Quality Assurance of Concrete Pavement*; NDOR Project Number P307, FINAL REPORT; University of Nebraska-Lincoln: Lincoln, NE, USA, 2009.
- [7] Maierhofer, C. Nondestructive Evaluation of Concrete Infrastructure with Ground Penetrating Radar. *ASCE J. Mater. Civil Eng.* **2003**, *15*, 287–297.
- [8] Hasan, M.I.; Yazdani, N. Ground penetrating radar utilization in exploring inadequate concrete covers in a new bridge deck. *Case Stud. Construct. Mater.* **2014**, *1*, 104–114.
- [9] Clark, M.; McCann, D.; Forde, M. Application of infrared thermography to the non-destructive testing of concrete and masonry bridges. *NDT&E Int.* **2003**, *36*, 265–275.
- [10] Maierhofer, C.; Arndt, R.; Röllig, M.; Rieck, C.; Walther, A.; Scheel, H.; Hillemeier, B. Application of impulse-thermography for non-destructive assessment of concrete structures. *Cem. Concr. Compos.* **2006**, *28*, 393–401.
- [11] Martz, H.; Roberson, G.; Skeate, M.; Schneberk, D.; Azevedo, S. Computerized tomography studies of concrete samples. *Nucl. Instrum. Methods Phys. Res. Sect. B Beam Interact. Mater. Atoms* **1991**, *58*, 216–226.
- [12] Martz, H.; Scheberk, D.; Roberson, G.; Monteiro, P. Computerized tomography analysis of reinforced concrete. *ACI Mater. J.* **1993**, *90*, 259–264.
- [13] Paetsch, O.; Baum, D.; Ehrig, K.; Meinel, D.; Prohaska, S. Automated 3D Crack Detection for Analyzing Damage Processes in Concrete with Computed Tomography. In Proceedings of the ICT Conference Wels 2012, Wels, Austria, 19–21 September 2012; pp. 321–330.
- [14] Paetsch, O.; Baum, D.; Prohaska, S.; Ehrig, K.; Meinel, D.; Ebell, G. 3D Corrosion Detection in Time-dependent CT Images of Concrete. In Proceedings of the Digital Industrial Radiology and Computed Tomography (DIR 2015), Ghent, Belgium, 22–25 June 2015.
- [15] Chady, T.; Enokizono, M. Flaw Reconstruction using a Multi-Frequency Method and an Artificial Intelligence. *JSAEM Stud. Appl. Electromagn. Mech.* **1999**, *8*, 203–208.
- [16] Chady, T.; Enokizono, M. Multi-frequency exciting and spectrogram based ECT method. *J. Magn. Magn. Mater.* **2000**, *215–216*, 700–703
- [17] Chady, T.; Łopato, P. Flaws Identification Using Eddy Current Differential Transducer and Artificial Neural Networks. In *Review of Quantitative Nondestructive Evaluation*; Thompson, D.O., Chimenti, D.E., Eds.; American Institute of Physics, AIP CP 820: Melville, NY, USA, 2005; Volume 25, pp. 783–790
- [18] Berowski, P.; Filipowicz, S.F.; Sikora, J.; Wójtowicz, S. Determining Location of Moisture Area of the Wall by 3D Electrical Impedance Tomography. In Proceedings of the 4th World Congress on Industrial Process Tomography, Aizu, Japan, 2–5 September 2005.
- [19] Seppänen, A.; Hallaji, M.; Pour-Ghaz, M. Electrical impedance tomography-based sensing skin for detection of damage in concrete. In Proceedings of the 11th European Conference on Non-Destructive Testing (ECNDT 2014), Prague, Czech Republic, 6–10 October 2014.
- [20] Karhunen, K.; Seppänen, A.; Lehtikoinen, A.; Monteiro, P.J.M.; Kaipio, J.P. Electrical resistance tomography imaging of concrete. *Cem. Concr. Res.* **2010**, *40*, 137–145.
- [21] Szymanik, B.; Frankowski, P.K.; Chady, T.; John Chelliah, C.R.A. Detection and Inspection of Steel Bars in Reinforced Concrete Structures Using Active Infrared Thermography with Microwave Excitation and Eddy Current Sensors. *Sensors* **2016**, *16*, 234.
- [22] Keo, S. A.; Brachelet, F.; Breaban, F.; Defer, D. Steel Detection in Reinforced Concrete Wall by Microwave Infrared Thermography. *NDT & E International* **2014**, *62*, 172–177. <https://doi.org/10.1016/j.ndteint.2013.12.002>.
- [23] Keo, S. A.; Brachelet, F.; Defer, D.; Breaban, F. Defects Detection by Infrared Thermography with a New Microwave Excitation System. *Mechanics & Industry* **2014**, *15* (6), 509–516. <https://doi.org/10.1051/meca/2014054>.
- [24] Keo, S. A. Développement d'une méthode de thermographie infrarouge active par excitation micro-ondes appliquée au contrôle non destructif. PhD thesis (in French), Université d'Artois, Béthune, France, 2013.
- [25] Maldague, X. P. V. *Theory and Practice of Infrared Technology for Nondestructive Testing*; New York, USA, 2001; Vol. Wiley series in microwave and optical engineering.
- [26] Kong, J. A. *Electromagnetic Wave Theory*; EMW Publishing: Cambridge: MA, USA, 2000.